

## Effects of high-entropy alloy binders on the microstructure and mechanical/thermal properties of cemented carbides

Jialin Sun, Xiao Li, Le Zhao, and Jun Zhao

Cite this article as:

Jialin Sun, Xiao Li, Le Zhao, and Jun Zhao, Effects of high-entropy alloy binders on the microstructure and mechanical/thermal properties of cemented carbides, *Int. J. Miner. Metall. Mater.*, 32(2025), No. 5, pp. 1190-1197. <https://doi.org/10.1007/s12613-024-2942-4>

View the article online at [SpringerLink](#) or [IJMMM Webpage](#).

### Articles you may be interested in

Andries Mthisi, Nicholas Malatji, A. Patricia, I. Popoola, and L. Rudolf Kanyane, [Parametric study of spark plasma sintering of  \$\text{Al}\_{20}\text{Cr}\_{20}\text{Fe}\_{25}\text{Ni}\_{25}\text{Mn}\_{10}\$  high entropy alloy with improved microhardness and corrosion](#), *Int. J. Miner. Metall. Mater.*, 29(2022), No. 1, pp. 119-127. <https://doi.org/10.1007/s12613-020-2200-3>

Xu Yang, Dezhi Chen, Li Feng, Gang Qin, Shiping Wu, and Ruirun Chen, [Enhancing the mechanical properties of casting eutectic high-entropy alloys via W addition](#), *Int. J. Miner. Metall. Mater.*, 31(2024), No. 6, pp. 1364-1372. <https://doi.org/10.1007/s12613-024-2892-x>

Na Xiao, Xu Guan, Dong Wang, Haile Yan, Minghui Cai, Nan Jia, Yudong Zhang, Claude Esling, Xiang Zhao, and Liang Zuo, [Impact of W alloying on microstructure, mechanical property and corrosion resistance of face-centered cubic high entropy alloys: A review](#), *Int. J. Miner. Metall. Mater.*, 30(2023), No. 9, pp. 1667-1679. <https://doi.org/10.1007/s12613-023-2641-6>

Yongchul Yoo, Xiang Zhang, Fei Wang, Xin Chen, Xing-Zhong Li, Michael Nastasi, and Bai Cui, [Spark plasma sintering of tungsten-based WTaVCr refractory high entropy alloys for nuclear fusion applications](#), *Int. J. Miner. Metall. Mater.*, 31(2024), No. 1, pp. 146-154. <https://doi.org/10.1007/s12613-023-2711-9>

Deyin Zhang, Xu Hao, Baorui Jia, Haoyang Wu, Lin Zhang, Mingli Qin, and Xuanhui Qu, [Influences of oxide content and sintering temperature on microstructures and mechanical properties of intragranular-oxide strengthened iron alloys prepared by spark plasma sintering](#), *Int. J. Miner. Metall. Mater.*, 30(2023), No. 9, pp. 1748-1755. <https://doi.org/10.1007/s12613-023-2631-8>

Zhuo Cheng, Shuize Wang, Guilin Wu, Junheng Gao, Xusheng Yang, and Honghui Wu, [Tribological properties of high-entropy alloys: A review](#), *Int. J. Miner. Metall. Mater.*, 29(2022), No. 3, pp. 389-403. <https://doi.org/10.1007/s12613-021-2373-4>




IJMMM WeChat



QQ author group

# Effects of high-entropy alloy binders on the microstructure and mechanical/thermal properties of cemented carbides

Jialin Sun<sup>1,2,3</sup>,, Xiao Li<sup>4</sup>, Le Zhao<sup>4</sup>, and Jun Zhao<sup>5</sup>

1) School of Mechanical, Electrical & Information Engineering, Shandong University, Weihai 264209, China

2) Shenzhen Research Institute of Shandong University, Shenzhen 518057, China

3) State Key Laboratory of Solid Lubrication, Lanzhou Institute of Chemical Physics, Chinese Academy of Sciences, Lanzhou 730000, China

4) Weihai Weiyang Tool Co., Ltd., Weihai 264210, China

5) Key Laboratory of High Efficiency and Clean Mechanical Manufacture of MOE, School of Mechanical Engineering, Shandong University, Jinan 250061, China

(Received: 26 March 2024; revised: 14 May 2024; accepted: 22 May 2024)

**Abstract:** The binder phase performs critically on the comprehensive properties of cemented carbides, especially the hardness (HV) and fracture toughness ( $K_{IC}$ ) relationship. There are strong motivations in both research community and industry for developing alternative binders to Co in cemented carbide system, due to the reasons such as price instability, property degeneration, and toxicity. Herein, six kinds of high entropy alloys (HEA) including CoCrFeNiMn, CoCrFeMnAl, CoCrFeNiAl, CoCrNiMnAl, CoFeNiMnAl, and CrFeNiMnAl were employed as the alternative binder for the preparation of WC–HEA cemented carbides through mechanical alloying and two-step spark plasma sintering. The impacts of HEA on the microstructures, mechanical properties, and thermal conductivity of WC–HEA hardmetals were determined and discussed. WC–HEA hardmetals exhibited both superior HV and  $K_{IC}$  to WC–metal or WC–intermetallic cemented carbides, indicating that HEA alloys were not only harder but also tougher in comparison with traditional metal or intermetallic binders. The HEA bonded hardmetals yielded thermal conductivities much lower than that of traditional WC–Co cemented carbide. The excellent HV– $K_{IC}$  relationship of WC–HEA facilitated the potential engineering structural application of cemented carbides.

**Keywords:** cemented carbide; high entropy alloy binder; two-step spark plasma sintering; mechanical properties; thermal conductivity

## 1. Introduction

Cemented carbides, also named as hardmetals, were considered as one of the most successful engineering composite materials by means of powder metallurgy since it was firstly developed by Karl Schroeter in 1923, which has been widely used as metal and wood machining tools, moulds, as well as wear-resistant mechanical parts [1–3]. Generally, cemented carbide is essentially a composite of hard carbide phase and soft metal phase. The carbide phase is responsible to the high hardness, while the metal phase critically influences the fracture toughness of cemented carbide. It is the combination of hardness and fracture toughness that makes the cemented carbide system uniquely different from either brittle ceramics or ductile metal alloys. Specifically, the cemented carbide is tougher and more impact resistance than ceramic matrix, whereas it is much harder in comparison with metal alloys. The metallic binder plays a critical role for cemented carbide achieving superior combination of mechanical properties.

In the past decades, the metal Co has been considered as the most popular binder phase for cemented carbide, as a function of the excellent wettability of Co on WC, high yield

strength and work hardening ability of Co, the plasticity of Co in the system, as well as the interfacial strength between Co and WC [4–6]. However, because of the combined influence of raising cost, hardness/corrosion/oxidation resistances deterioration, and negative effects on health, there is a strong motivation in both academia and industry for investigating alternative binder to Co in cemented carbides [7–8]. In other words, the design of WC–Co materials must balance a host of properties with respect to the intended applications. Up to now, metal, intermetallic compound, and ceramics (metal carbide and oxide) have been used to replace Co in cemented carbide systems [9–14]. However, whilst initially appealing, none of them, to date has been commercialized and produced on an industrial scale. Generally, the WC–metal exhibited unsatisfactory hardness and wear resistance, while WC–intermetallic and WC–ceramics yielded poor fracture toughness. For example, WC–9.6wt%Ni–0.4wt%Co possessed an excellent fracture toughness of  $12.5 \text{ MPa} \cdot \text{m}^{1/2}$  with a poor hardness of 11.6 GPa [15], whereas WC–10vol%  $\text{Fe}_3\text{Al}$  and WC–10wt%  $\text{Al}_2\text{O}_3$  exhibited high hardness of 24.1 and 20 GPa but inferior fracture toughness of 7.5 and 5.9  $\text{MPa} \cdot \text{m}^{1/2}$  [16–17]. Advanced alternative binder to Co should

 Corresponding author: Jialin Sun E-mail: [sunjialin@sdu.edu.cn](mailto:sunjialin@sdu.edu.cn)

© University of Science and Technology Beijing 2025

be effective not only in facilitating the densification of WC, but also overcoming the balance between hardness and fracture toughness of cemented carbides.

Very recently, high entropy alloy (HEA), also named as multiple principal element alloy or compositionally complex alloy, has been attempted to be employed as the rather potential substitute binder for Co in cemented carbides, due to its superior thermal stability, room/high temperature mechanical properties, and wear/oxidation/corrosion resistances compared to traditional metal alloys, resulting from the properties of high entropy effect, severe lattice distortion, slow diffusion, and “cocktail effect” [7,18]. The excellent wettability with a contact angle of less than  $5^\circ$  of HEA on WC could be achieved through regulating the element of HEA. For example, Cr was proved to be an active element for the wetting of HEA/WC system through adsorbing at the interface during wetting [19]. It was proposed by Chen *et al.* [20] that the HEA was effective in inhibiting the grain growth of WC, consequently endowing the WC–HEA superior mechanical properties to the traditional WC–Co alloys. Zhou *et al.* [21] reported that WC–HEA possessed significantly enhanced corrosion resistance in comparison with conventional WC–Co cemented carbides. Luo *et al.* [22] demonstrated that the improved oxidation resistance of WC–HEA was ascribed to the outstanding anti-oxidation nature of HEA. In other words, the selective oxidation occurrence of HEA binder effectively inhibited the inward diffusion of oxygen to the interface between the oxide layer and the matrix. Holmström *et al.* [23] suggested that the HEA bonded cemented carbide could withstand much higher machining speeds in comparison with traditional hardmetal with Co binder, as a function of the excellent plastic deforming resistance of HEA during the high-speed cutting process. On the other hand, Linder [24] illustrated that the preparation of high dense WC–HEA with single-phase HEA was rather challenging for the generally required long ball-milling process and high temperature sintering.

In the present work, WC–HEA cemented carbides were prepared via mechanical alloying followed by two-step spark plasma sintering (SPS) employing various HEA binders including CoCrFeNiMn, CoCrFeMnAl, CoCrFeNiAl, CoCrNiMnAl, CoFeNiMnAl, and CrFeNiMnAl. The influence of binder phase on the phase composition, microstructure, mechanical properties, and thermal conductivity of WC–HEA was investigated and discussed in detail. This study can provide reference for the development of high-performance cemented carbides with alternative binder to Co.

## 2. Experimental

### 2.1. Material preparation

Al, Co, Cr, Fe, Mn, and Ni powders ( $0.5\ \mu\text{m}$ , 99.9% purity) were employed in this study for the synthesis of high entropy alloy binders including CoCrFeNiMn, CoCrFeMnAl, CoCrFeNiAl, CoCrNiMnAl, CoFeNiMnAl, and CrFeNiMnAl. For certain HEA, five metal powders were firstly weighted in an equimolar ratio, subjected to homogenization

by combined ultrasonication and mechanical stirring in absolute alcohol for 1 h using polyethyleneglycol (PEG) as the dispersant, subsequently followed by 24 h ball-milling process under an Ar atmosphere employing a high energy planetary ball-milling machine. Finally, the HEA slurries were dried and screened, obtaining the HEA binder powders. The WC powders ( $0.4\ \mu\text{m}$ , 99.9% purity) were mixed with the HEA powders. Further homogenization was performed through ultrasonic dispersion and ball milling. In the following step, the hybrid slurries were dried and screened, obtaining six kinds of WC–HEA including WC–6wt%CoCrFeNiMn (WH1), WC–6wt%CrFeNiMnAl (WH2), WC–6wt%CoFeNiMnAl (WH3), WC–6wt%CoCrNiMnAl (WH4), WC–6wt%CoCrFeMnAl (WH5), and WC–6wt%CoCrFeNiAl (WH6). The reference WC–6wt%Co was also prepared employing the same conditions.

### 2.2. Two-step spark plasma sintering

In our previous studies, two-step sintering has been proved to be an effective method for improving the densification and homogeneous distribution of components in high-entropy materials without causing grain growth [25–26]. Based on two-step sintering methodology, the green body was firstly heated to a relatively high temperature with rather short or without soaking time, then cooled to a low temperature with long holding time. The densification process of WC–HEA was carried out in a spark plasma sintering system with the two-step sintering parameters as illustrated in Fig. 1.

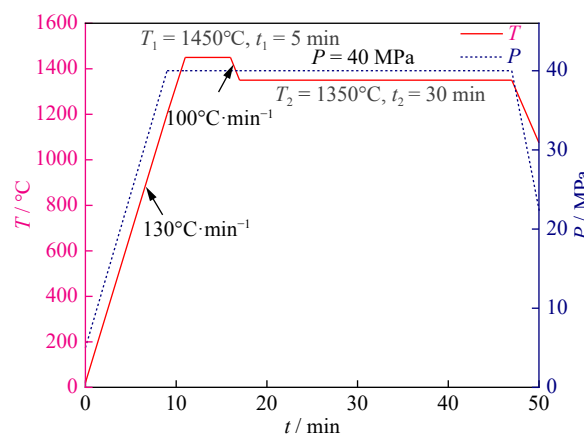


**Fig. 1.** Two-step spark plasma sintering process for the WC–HEA cemented carbides.  $T$ ,  $P$ , and  $t$  represent sintering temperature, pressure, and time, respectively.

### 2.3. Microstructure and properties characterization

The density of samples was determined through the Archimedes principle with distilled water as the immersion medium employing an analytical balance. The hardness measurements were operated on a Vickers hardness tester with a load of 294 N and dwell time of 10 s at room temperature. The fracture toughness was evaluated via both the indentation method and single-edge notched beam method (SENB). The indentation fracture toughness was determined by the following expression:

$$K_{IC} = 0.0889 \times \sqrt{\frac{HV_{30} \times F}{l}} \quad (1)$$

where  $K_{IC}$  is the fracture toughness ( $\text{MPa} \cdot \text{m}^{1/2}$ ),  $HV_{30}$  is the hardness (GPa),  $F$  is the applied force (N), and  $l$  is the total length of the four cracks (mm). SENB test was performed on the specimens ( $3 \text{ mm} \times 4 \text{ mm} \times 20 \text{ mm}$ ) with a span of 16 mm at a cross-head speed of  $0.05 \text{ mm} \cdot \text{min}^{-1}$  using three point bending method. All values reported in this paper represent the average of at least five measurements per configuration. The SENB fracture toughness was calculated according to the following equations [27]:

$$K_{IC} = \left( \frac{F_{\max} \times L \times 10^{-6}}{W \times B^{3/2}} \right) f\left(\frac{a}{B}\right) \quad (2)$$

$$f\left(\frac{a}{B}\right) = \frac{3\left(\frac{a}{B}\right)^{\frac{1}{2}} \left[ 1.99 - \left(\frac{a}{B}\right) \left(1 - \frac{a}{B}\right) \left( 2.15 - 3.93 \frac{a}{B} + 2.7 \left(\frac{a}{B}\right)^2 \right) \right]}{2 \left( 1 + \frac{2a}{B} \right) \left( 1 - \frac{a}{B} \right)^{\frac{3}{2}}} \quad (3)$$

where  $K_{IC}$  is the fracture toughness ( $\text{MPa} \cdot \text{m}^{1/2}$ ),  $F_{\max}$  is the maximum force (N),  $L$  is the support span (m),  $W$  is the width of the sample (m),  $B$  is the height of the sample (m), and  $a$  is the depth of notch (m). Thermal diffusivity measurement was undertaken for samples  $10 \text{ mm}$  (length)  $\times$   $10 \text{ mm}$  (width)  $\times$   $1.6 \text{ mm}$  (thickness) on a laser flash unit under atmospheric conditions. The measurements were repeated 5 times and exhibited excellent reproducibility. Thermal conductivity  $\lambda$  ( $\text{W} \cdot \text{m}^{-1} \cdot \text{K}^{-1}$ ) was then calculated from the following equation:

$$\lambda = \alpha \times \rho \times C_p \quad (4)$$

where  $\alpha$  is the thermal diffusivity in  $\text{mm}^2 \cdot \text{s}^{-1}$ ,  $\rho$  is the density in  $\text{g} \cdot \text{cm}^{-3}$ , and  $C_p$  is the specific heat capacity in  $\text{J} \cdot \text{g}^{-1} \cdot \text{K}^{-1}$  and measured employing a differential scanning calorimeter. Samples for phase and microstructural evaluation were carefully prepared using standard metallographic preparation procedures. The phase composition characterization of the WC-HEA was carried out employing an X-ray diffraction (XRD) system, operated with a Cu  $K_\alpha$  source at an angle range of  $30^\circ$  to  $90^\circ$ . The microstructure was examined using a scanning electron microscope (SEM) and transmission electron microscope (TEM) equipped with an energy-dispersive X-ray spectroscopy (EDS) system.

## 3. Results and discussion

### 3.1. Phases composition

Fig. 2 illustrated the XRD patterns of different HEA bonded cemented carbide powder mixtures before and after the two-step SPS process. There was no significant difference in the XRD patterns of samples with various HEA binder. The reflections associated with the WC phase were clearly visible for all samples. With respect to HEA, the ball-milled

WC-HEA powders exhibited hybrid body-centered cubic (bcc) and face-centered cubic (fcc) structure solid solution instead of single-phase HEA, while the two-step SPSed samples yielded all fcc structure, indicating the structural transformation of HEA from bcc to fcc during the sintering process. The structural transformation at high temperature is associated with the metastable state of the bcc structure formed during the ball-milling process. In other words, the metastable bcc solid solutions tend to transform into more thermodynamically stable fcc solid solutions during the sintering process [28]. Furthermore, it should be noted that no  $\text{W}_2\text{C}$ ,  $\eta$ -phase, metal oxides, or other secondary phase was detected in the XRD patterns of either ball-milled powders or sintered specimens, which is helpful in improving the mechanical responses of WC-HEA. The absence of these detrimental secondary phase suggests no significant alloying reaction between WC and HEA during the preparing process, which is attributed to the two-step SPS containing rather short soaking time at high temperature.

### 3.2. Microstructure and mechanical properties

The two-phase microstructure of the sintered bulk WC-HEA was further confirmed by determining the distribution of elemental composition through SEM and EDS, as shown in Fig. 3. It was noted that the five elements in the HEA binder were homogeneously distributed throughout the bulk specimens, regardless of the kinds of HEA. No apparent precipitation observed, suggesting that the two-step SPS process effectively facilitated the uniform distribution of the microstructure. Regarding the first-step sintering, conducted at high temperature with short holding time, as the liquid phase sintering, the increased activation energy and diffusion capacity acted critically on improving the distribution of HEA elements. During the first-step sintering at  $1450^\circ\text{C}$ , some liquid HEAs formed, which has been claimed by many previous studies about WC-HEA cemented carbides [29–30]. Actually, the metal point of HEA is much lower than  $1450^\circ\text{C}$ . For example, the melting point of FeCoNiCrMn has been proved to be around  $1406^\circ\text{C}$  [31]. The liquid HEA is helpful in contributing to the densification of WC-HEA. However, much liquid HEA would result in the abnormal grain growth of the WC. Therefore, the holding time at first-step sintering was set rather short. The second-step sintering, conducted at low temperature with rather long soaking time, was solid-phase sintering that significantly enhanced the atomic inter-diffusion driven by the concentration gradient. Additionally, no obvious micropores were observed for all WC-HEA samples, indicating the high densification through two-step SPS as shown in Fig. 4. Taking WC-HEA as an example, the TEM image and STEM-EDS mappings were performed to determine the nano and atomic level microstructures of HEA binders, as illustrated in Fig. 5. It is noted that Fe, Co, Ni, Cr, and Mn were homogeneously distributed at the nanometer scale.

The hard phase WC exhibited narrow grain size corresponding to the initial grain size, suggesting the grain growth inhibition effect of HEA, which could effectively improve



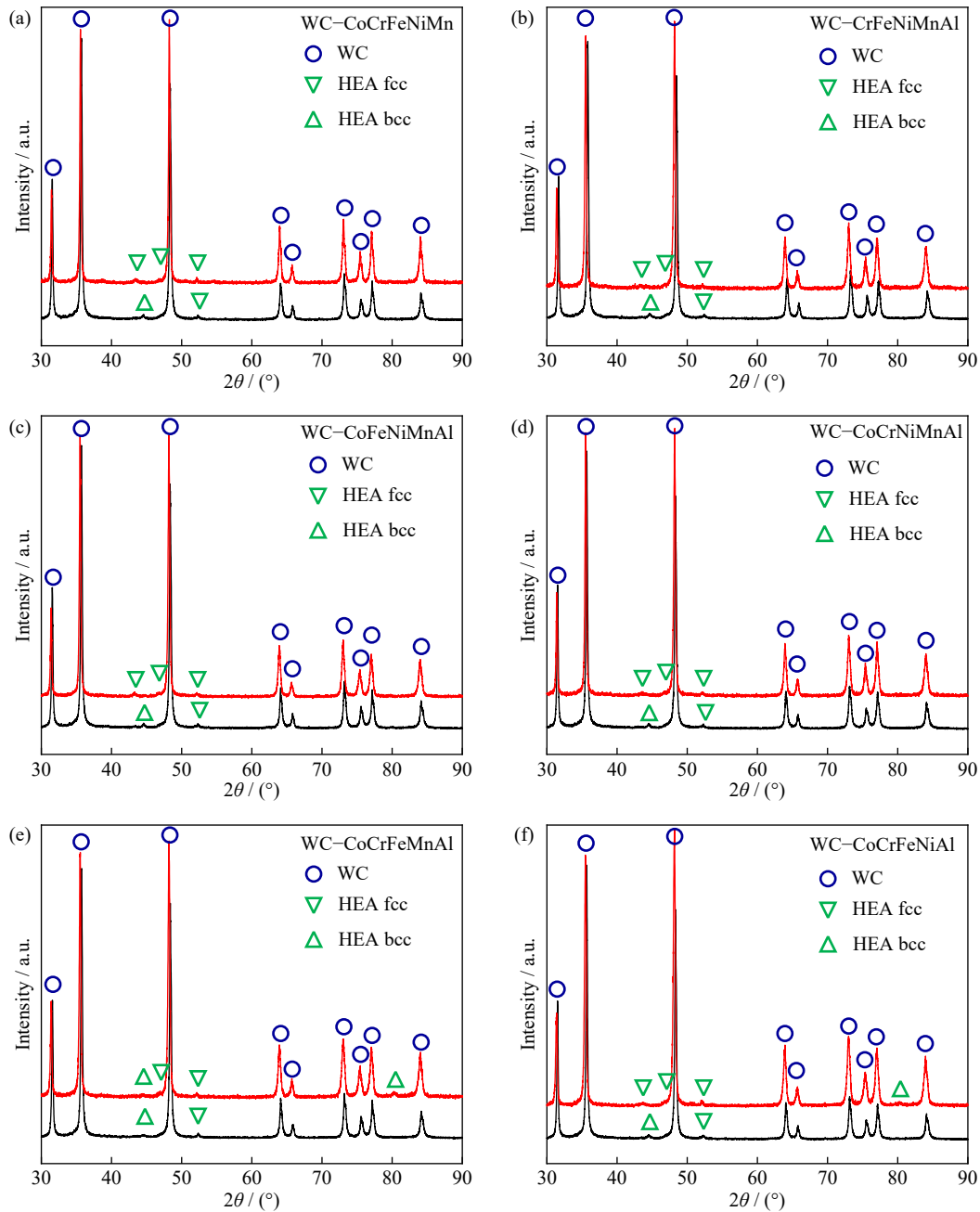


**Fig. 2.** XRD patterns of powders (red line) and the sintered samples (black line): (a) WC-6wt%CoCrFeNiMn, (b) WC-6wt%CrFeNiMnAl, (c) WC-6wt%CoFeNiMnAl, (d) WC-6wt%CoCrNiMnAl, (e) WC-6wt%CoCrFeMnAl, and (f) WC-6wt%CoCrFeNiAl.

the performance of cemented carbide. For one thing, much greater barrier must be overcome for the grain growth of WC as a function of the sluggish diffusion effect of HEAs. Moreover, it is proposed that the diffusion rate of multi-element HEA was determined by the element with highest diffusion activation energy [32–33]. For another, the lattice distortion of HEA results in the inhomogeneous of the crystal structure and changes the angles and distances between atoms, which in turn suppresses grain growth. Besides, the grain growth of WC results from the dissolution and proliferation process, which is closely associated with the chemical composition of the surrounding WC grains. The chemical elements of the HEA generate different interfacial energies between the WC and the matrix, causing the W and C elements to encounter different energy barriers to diffusion.

This, in turn, significantly inhibited the grain growth. Therefore, though without grain growth inhibitor doping, the final WC-HEAs were free of grain growth. Furthermore, the fracture modes of the as-prepared WC-HEA exhibited a hybrid of transgranular fracture and intergranular fracture, implying the high bonding strength between WC and HEA. Besides, matrix tearing and dimple were observed in the fracture surface as demonstrated in Fig. 3.

The hardness (HV) and fracture toughness ( $K_{IC}$ ) of cemented carbides with different binders are presented in Fig. 6. The hardness of the base WC-Co was found to be 17.6 GPa, while the HEA bonded cemented carbides yielded hardness between 22.7 to 24.3 GPa. The outstanding hardness of WC-HEA is attributed to the superior grain growth inhibition effect and higher hardness of HEA in comparison with

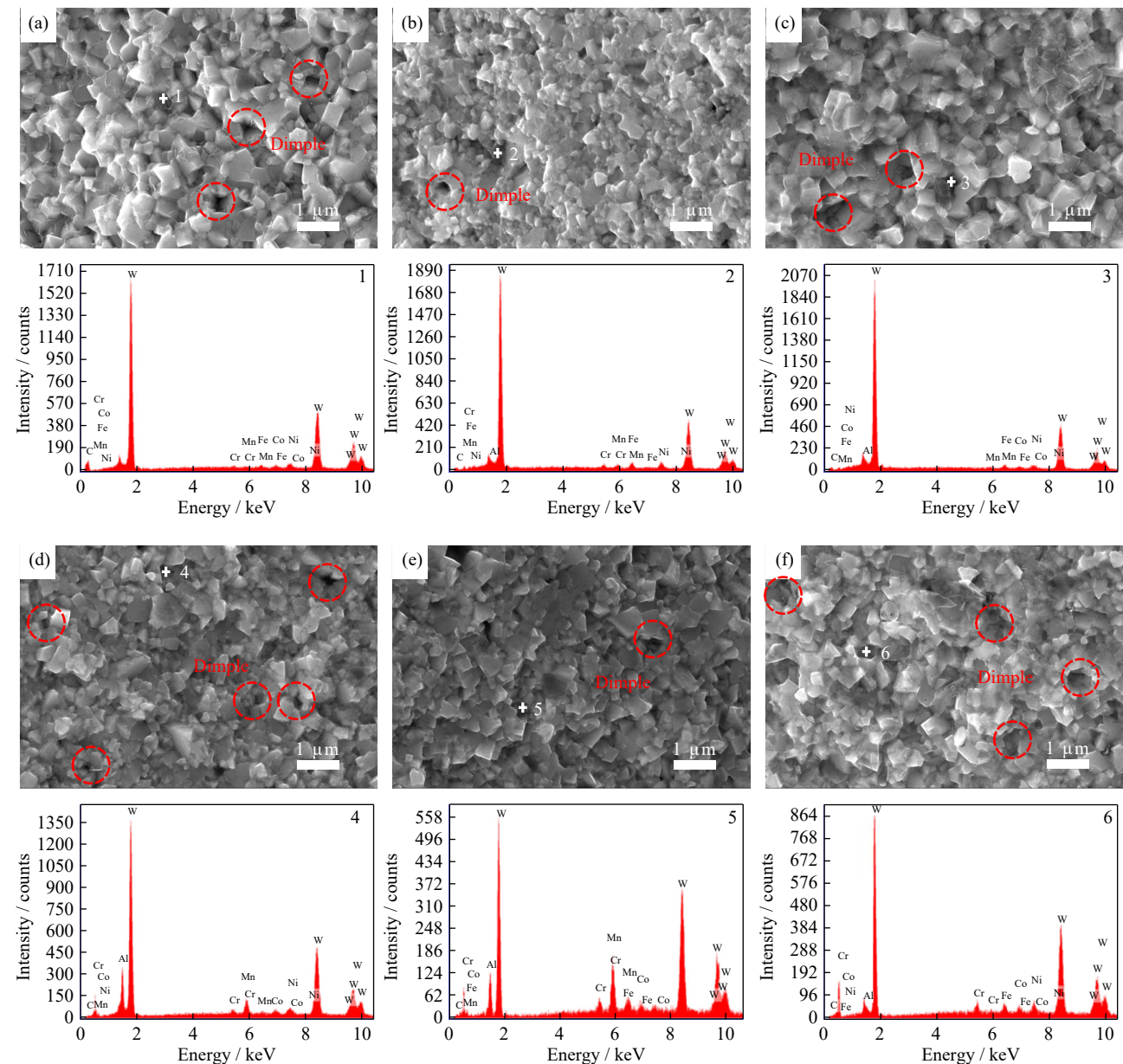


**Fig. 3.** SEM images and EDS analyses illustrating the fracture surface of WC-HEA cemented carbides obtained through two-step SPS: (a) WC-6wt%CoCrFeNiMn, (b) WC-6wt%CrFeNiMnAl, (c) WC-6wt%CoFeNiMnAl, (d) WC-6wt%CoCrNiMnAl, (e) WC-6wt%CoCrFeMnAl, and (f) WC-6wt%CoCrFeNiAl.

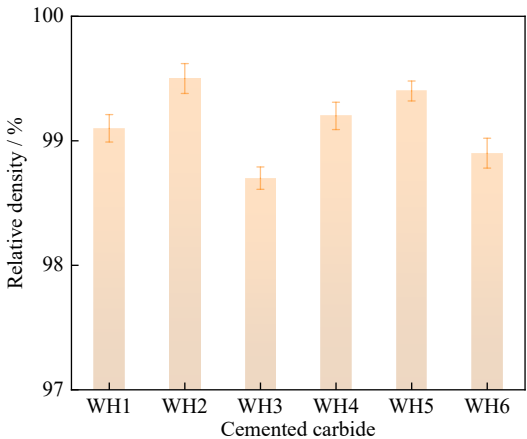


**Fig. 4.** Relative density of WC-HEA samples obtained by two-step sintering.

Co. The fracture toughness was evaluated through both indentation and SENB tests. From the results obtained, the indentation fracture toughness of WC-HEA varied from 12.4 to 13.6 MPa·m<sup>1/2</sup>, and the SENB fracture toughness was between 11.9 and 16.6 MPa·m<sup>1/2</sup>, depending on the kinds of HEA binders, which were higher than those of the base WC-Co hardmetal prepared through the same conditions. The main reason for the enhanced fracture toughness of WC-HEA is that the fcc structural HEA possessed much better plasticity comparing with traditional hcp structural Co. The fcc structural binder facilitated the generation of sliding systems, thus slowing down the unidirectional crack propagation. Therefore, it is clearly that the as-prepared WC-HEA composites exhibited simultaneously enhanced hardness and fracture toughness in comparison with traditional WC-Co cemented carbides. Fig. 7 illustrates the frac-

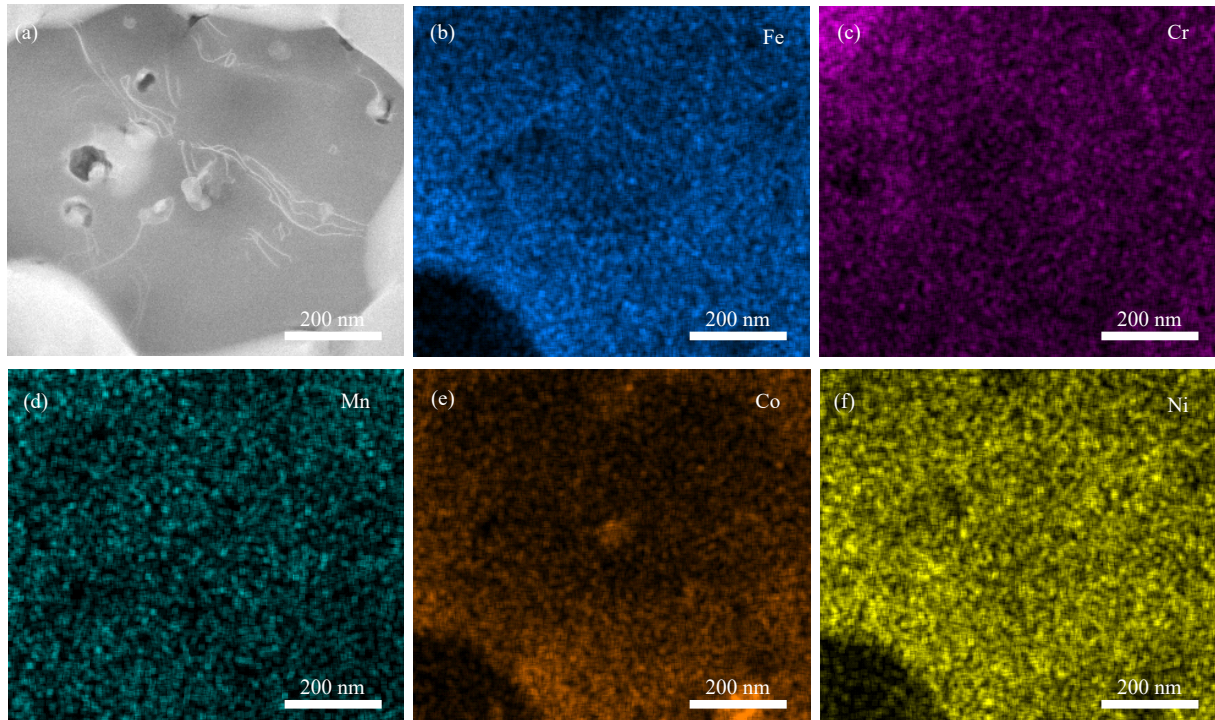


Fig. 5. TEM images and corresponding STEM-EDS elemental mappings of FeCoNiCrMn binders.

ture surface of WH4 and WH6 after SENB tests. It is noted that the WC-HEA samples yielded a rather tortuous crack propagation path with obvious crack deflection, which is consist with the high fracture toughness values as demonstrated in Fig. 6.

It is well known that the hardness and fracture toughness are the most important mechanical response for cemented carbide system. The binders critically imparted the balance of hardness and fracture toughness of hardmetals. Fig. 8 is a comparative plot of hardness and fracture toughness of as-prepared WC-HEA composites and literature reported WC-metal composites (including WC-Co, WC-Fe, WC-Ni, WC-FeMn, and WC-Al), WC-intermetallic composites (such as WC-FeAl and WC-Ni<sub>3</sub>Al), and other WC-HEA composites [21–43]. The trade-off relationships were noted between hardness and toughness for both WC-metal and WC-intermetallic systems, which was not obvious in case of

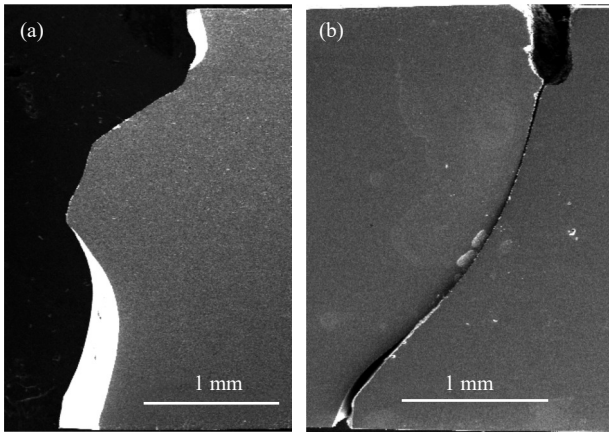


Fig. 7. Fracture surfaces of WH4 (a) and WH6 (b) after SENB tests.

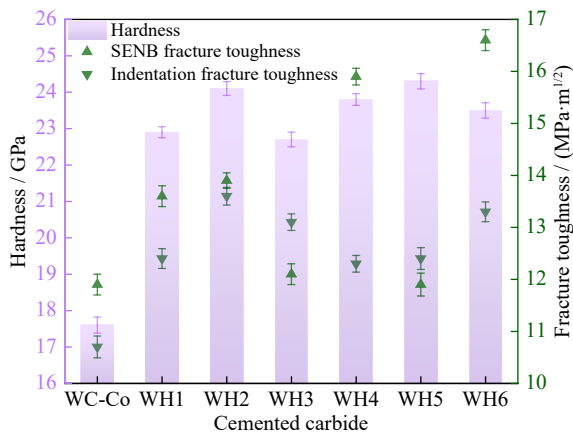


Fig. 6. Hardness and fracture toughness of different HEA bonded cemented carbides and the reference WC-Co.

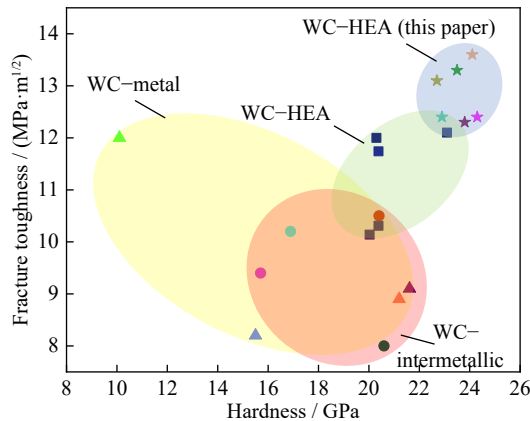


Fig. 8. Hardness and fracture toughness relation for as-prepared WC-HEA and literature reported WC-metal (including WC-Co, WC-Fe, WC-Ni, WC-FeMn, and WC-Al), WC-intermetallic (such as WC-FeAl and WC-Ni<sub>3</sub>Al), and other WC-HEA [21,34–43].



WC–HEA system. Clustered to the upper right region of the diagram, WC–HEA hardmetals exhibited both superior hardness and fracture toughness compared to WC–metal or WC–intermetallic cemented carbides, indicating that HEA alloys were not only harder but also tougher in comparison with traditional metal or intermetallic binders. The excellent  $HV-K_{IC}$  relationship of WC–HEA would significantly facilitate the potential engineering structural application of cemented carbides.

### 3.3. Thermal conductivity

Thermal conductivity characterizes the material's ability to conduct heat, which is also rather significant for the service life of cemented carbide products. Thus, thermal conductivity was measured at both room temperature and high temperature to evaluate the impact of HEA on the heat conduction of hardmetal materials, as demonstrated in Fig. 9. Obviously, HEA bonded cemented carbides yielded significantly lower thermal conductivities than traditional WC–Co at both room temperature and high temperature. Taking the room temperature as an example, the base WC–Co cemented carbide exhibited a thermal conductivity of  $89.7 \text{ W} \cdot \text{m}^{-1} \cdot \text{K}^{-1}$ , while the HEA bonded hardmetals yielded thermal conductivities ranging from 46.3 to  $72.7 \text{ W} \cdot \text{m}^{-1} \cdot \text{K}^{-1}$ , indicating the significant effect of binder phase on the thermal conductivity of cemented carbides. There are several reasons contributing to the decreased thermal conductivity of WC–HEA hardmetals in comparison with WC–Co cemented carbides. For one thing, HEA possesses lower thermal conductivity than Co, resulting from the severe anion sublattice distortions accompanying the formation of the solid solution. Furthermore, HEA yields superior grain growth inhibition effect to Co, resulting in smaller WC grain size in WC–HEA than WC–Co system. Besides, the interface thermal resistance in WC–HEA system is higher than in WC–Co system, because of the some better wettability of Co on WC than HEA.

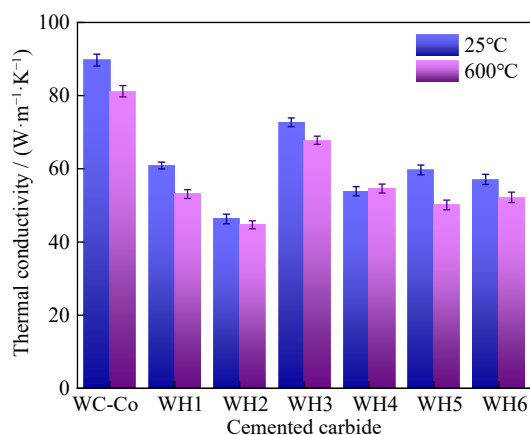


Fig. 9. Effect of different binders on the thermal conductivity of cemented carbides.

## 4. Conclusions

The current study applies towards investigate the influ-

ences of HEA on the microstructures, mechanical properties, and thermal conductivity of WC-based hardmetals.

(1) With respect to HEA, the ball-milled WC–HEA powders exhibited hybrid bcc and fcc structure solid solution, while the two-step SPSed samples yielded all fcc structure, indicating the structural transformation of HEA from bcc to fcc during the sintering process.

(2) The HEA bonded cemented carbides yielded hardness between 22.7 to 24.3 GPa, with an indentation fracture toughness of WC–HEA varied from 12.4 to  $13.6 \text{ MPa} \cdot \text{m}^{1/2}$  and SENB fracture toughness between 11.9 and  $16.6 \text{ MPa} \cdot \text{m}^{1/2}$ . WC–HEA hardmetals exhibited both superior hardness and fracture toughness compared to WC–metal or WC–intermetallic cemented carbides, indicating that HEA alloys were not only harder but also tougher in comparison with traditional metal or intermetallic binders.

(3) The base WC–Co cemented carbide exhibited a thermal conductivity of  $89.7 \text{ W} \cdot \text{m}^{-1} \cdot \text{K}^{-1}$ , whereas the HEA bonded hardmetals yielded thermal conductivities ranging from 46.3 to  $72.7 \text{ W} \cdot \text{m}^{-1} \cdot \text{K}^{-1}$  at room temperature, indicating the significant effect of binder phase on the thermal conductivity of cemented carbides.

## Acknowledgements

This work was financially supported by the National Natural Science Foundation of China (No. 52375451), the Shandong Provincial Natural Science Foundation, China (Nos. ZR2023YQ052 and ZR2023ME087), the Shandong Provincial Technological SME Innovation Capability Promotion Project, China (No. 2023TSGC0375), the Young Taishan Scholars Program of Shandong Province, China (No. tsqn202306041), the Guangdong Basic and Applied Basic Research Foundation, China (No. 2023A1515010044), the Shandong Provincial Youth Innovation Team, China (No. 2022KJ038), the Open project of State Key Laboratory of Solid Lubrication, China (No. LSL-22-11), and Qilu Youth Scholar Project Funding of Shandong University, China.

## Conflict of Interest

The authors declare that there is no conflict of financial or non-financial interests involved.

## References

- [1] G.S. Upadhyaya, Materials science of cemented carbides—An overview, *Mater. Des.*, 22(2001), No. 6, p. 483.
- [2] L. Prakash, Fundamentals and general applications of hardmetals, [in] D. Mari, L. Llanes, and V. K. Sarin, eds., *Comprehensive Hard Materials*, Elsevier, Amsterdam, 2014, p. 29.
- [3] R.M. Raihanuzzaman, Z.H. Xie, S.J. Hong, and R. Ghomashchi, Powder refinement, consolidation and mechanical properties of cemented carbides—An overview, *Powder Technol.*, 261(2014), p. 1.
- [4] L.Y. Shi, Y.M. Liu, J.H. Huang, S.Q. Zhang, and X.K. Zhao, Growth kinetics of cubic carbide free layers in graded cemented carbides, *Int. J. Miner. Metall. Mater.*, 19(2012), No. 1, p. 64.



- [5] J.L. Sun, J. Zhao, F. Gong, Z.L. Li, and X.Y. Ni, Design, fabrication and characterization of multi-layer graphene reinforced nanostructured functionally graded cemented carbides, *J. Alloy. Compd.*, 750(2018), p. 972.
- [6] J.L. Sun, Z.F. Huang, and J. Zhao, High-hard and high-tough WC–TiC–Co cemented carbide reinforced with graphene, *Mater. Today Commun.*, 29(2021), art. No. 102841.
- [7] B. Straumal and I. Konyashin, WC-based cemented carbides with high entropy alloyed binders: A review, *Metals*, 13(2023), No. 1, art. No. 171.
- [8] J.L. Sun, Y. Chen, P. Zhai, Y.H. Zhou, J. Zhao, and Z.F. Huang, Tribological performance of binderless tungsten carbide reinforced by multilayer graphene and SiC whisker, *J. Eur. Ceram. Soc.*, 42(2022), No. 12, p. 4817.
- [9] W.D. Schubert, M. Fugger, B. Wittmann, and R. Useldinger, Aspects of sintering of cemented carbides with Fe-based binders, *Int. J. Refract. Met. Hard Mater.*, 49(2015), p. 110.
- [10] J.M. Tarragó, C. Ferrari, B. Reig, D. Coureaux, L. Schneider, and L. Llanes, Mechanics and mechanisms of fatigue in a WC–Ni hardmetal and a comparative study with respect to WC–Co hardmetals, *Int. J. Fatigue*, 70(2015), p. 252.
- [11] A.M. Vilardeell, N. Cinca, E. Tarrés, and M. Kobashi, Iron aluminides as an alternative binder for cemented carbides: A review and perspective towards additive manufacturing, *Mater. Today Commun.*, 31(2022), art. No. 103335.
- [12] J.L. Sun, J. Zhao, M.J. Chen, X.C. Wang, X. Zhong, and G.M. Hou, Determination of microstructure and mechanical properties of functionally graded WC–TiC–Al<sub>2</sub>O<sub>3</sub>–GNPs micro-nano composite tool materials via two-step sintering, *Ceram. Int.*, 43(2017), No. 12, p. 9276.
- [13] K. Zhang, Z.J. Zhang, X.X. Lu, et al., Microstructure and composition of the grain/binder interface in WC–Ni<sub>3</sub>Al composites, *Int. J. Refract. Met. Hard Mater.*, 44(2014), p. 88.
- [14] X.Q. Li, M.A. Zhang, D.H. Zheng, T. Cao, J. Chen, and S.G. Qu, The oxidation behavior of the WC–10wt.% Ni<sub>3</sub>Al composite fabricated by spark plasma sintering, *J. Alloy. Compd.*, 629(2015), p. 148.
- [15] E.A. Almond and B. Roebuck, Identification of optimum binder phase compositions for improved WC hard metals, *Mater. Sci. Eng. A*, 105–106(1988), p. 237.
- [16] S.G. Huang, O. Van der Biest, and J. Vleugels, Pulsed electric current sintered Fe<sub>3</sub>Al bonded WC composites, *Int. J. Refract. Met. Hard Mater.*, 27(2009), No. 6, p. 1019.
- [17] D.H. Zheng, X.Q. Li, X. Ai, C. Yang, and Y.Y. Li, Bulk WC–Al<sub>2</sub>O<sub>3</sub> composites prepared by spark plasma sintering, *Int. J. Refract. Met. Hard Mater.*, 30(2012), No. 1, p. 51.
- [18] Y.G. Yan, D. Lu, and K. Wang, Overview: Recent studies of machine learning in phase prediction of high entropy alloys, *Tungsten*, 5(2023), No. 1, p. 32.
- [19] W.Y. Luo, Y.Z. Liu, and C. Tu, Wetting behaviors and interfacial characteristics of molten Al<sub>x</sub>CoCrCuFeNi high-entropy alloys on a WC substrate, *J. Mater. Sci. Technol.*, 78(2021), p. 192.
- [20] C.S. Chen, C.C. Yang, H.Y. Chai, J.W. Yeh, and J.L.H. Chau, Novel cermet material of WC/multi-element alloy, *Int. J. Refract. Met. Hard Mater.*, 43(2014), p. 200.
- [21] P.F. Zhou, D.H. Xiao, and T.C. Yuan, Comparison between ultrafine-grained WC–Co and WC–HEA-cemented carbides, *Powder Metall.*, 60(2017), No. 1, p. 1.
- [22] W.Y. Luo, Y.Z. Liu, X.H. Liu, and Z.G. Zhou, Oxidation behavior of ultrafine WC-based cemented carbides with Al<sub>x</sub>CoCrCuFeNi high-entropy alloy binders, *Ceram. Int.*, 47(2021), No. 6, p. 8498.
- [23] E. Holmström, R. Lizárraga, D. Linder, et al., High entropy alloys: Substituting for cobalt in cutting edge technology, *Appl. Mater. Today*, 12(2018), p. 322.
- [24] D. Linder, *High Entropy Alloys—Alternative Binders in Cemented Carbides* [Dissertation], Linköping University Department of Physics, Sweden, 2015, p. 1.
- [25] J.L. Sun, J. Zhao, Y.H. Zhou, et al., High-performance multi-functional (Hf<sub>0.2</sub>Nb<sub>0.2</sub>Ta<sub>0.2</sub>Ti<sub>0.2</sub>Zr<sub>0.2</sub>)C high-entropy ceramic reinforced with low-loading 3D hybrid graphene–carbon nanotube, *J. Adv. Ceram.*, 12(2023), No. 2, p. 341.
- [26] J.L. Sun, J. Zhao, Y. Chen, L. Wang, X.L. Yun, and Z.F. Huang, Toughening in low-dimensional nanomaterials high-entropy ceramic nanocomposite, *Composites Part B*, 231(2022), art. No. 109586.
- [27] J. Sun, P. Zhai, Y. Chen, J. Zhao, and Z. Huang, Hierarchical toughening of laminated nanocomposites with three-dimensional graphene/carbon nanotube/SiC nanowire, *Mater. Today Nano*, 18(2022), art. No. 100180.
- [28] I. Solodkyi, S. Teslia, O. Bezdorozhev, et al., Hardmetals prepared from WC–W<sub>2</sub>C eutectic particles and AlCrFeCoNiV high entropy alloy as a binder, *Vacuum*, 195(2022), art. No. 110630.
- [29] I.L. Velo, F.J. Gotor, M.D. Alcalá, C. Real, and J.M. Córdoba, Fabrication and characterization of WC–HEA cemented carbide based on the CoCrFeNiMn high entropy alloy, *J. Alloy. Compd.*, 746(2018), p. 1.
- [30] D.Q. Dong, X. Xiang, B. Huang, et al., Microstructure and properties of WC–Co/CrMnFeCoNi composite cemented carbides, *Vacuum*, 179(2020), art. No. 109571.
- [31] M.A. Gutierrez, G.D. Rodriguez, G. Bozzolo, and H.O. Mosca, Melting temperature of CoCrFeNiMn high-entropy alloys, *Comput. Mater. Sci.*, 148(2018), p. 69.
- [32] K.Y. Tsai, M.H. Tsai, and J.W. Yeh, Sluggish diffusion in Co–Cr–Fe–Mn–Ni high-entropy alloys, *Acta Mater.*, 61(2013), No. 13, p. 4887.
- [33] S. Yadav, Q.F. Zhang, A. Behera, et al., Role of binder phase on the microstructure and mechanical properties of a mechanically alloyed and spark plasma sintered WC–FCC HEA composites, *J. Alloy. Compd.*, 877(2021), art. No. 160265.
- [34] W.D. Schubert, H. Neumeister, G. Kinger, and B. Lux, Hardness to toughness relationship of fine-grained WC–Co hardmetals, *Int. J. Refract. Met. Hard Mater.*, 16(1998), No. 2, p. 133.
- [35] B. Wittmann, W.D. Schubert, and B. Lux, WC grain growth and grain growth inhibition in nickel and iron binder hardmetals, *Int. J. Refract. Met. Hard Mater.*, 20(2002), No. 1, p. 51.
- [36] C. Hanyaloglu, B. Aksakal, and J.D. Bolton, Production and indentation analysis of WC/Fe–Mn as an alternative to cobalt-bonded hardmetals, *Mater. Charact.*, 47(2001), No. 3–4, p. 315.
- [37] I.J. Shon, High-frequency induction-heated consolidation of nanostructured WC and WC–Al hard materials and their mechanical properties, *Int. J. Refract. Met. Hard Mater.*, 64(2017), p. 242.
- [38] R. Furushima, K. Katou, S. Nakao, et al., Relationship between hardness and fracture toughness in WC–FeAl composites fabricated by pulse current sintering technique, *Int. J. Refract. Met. Hard Mater.*, 42(2014), p. 42.
- [39] M.A. Zhang, Z. Cheng, J.M. Li, S.G. Qu, and X.Q. Li, Study on microstructure and mechanical properties of WC–10Ni<sub>3</sub>Al cemented carbide prepared by different ball-milling suspension, *Materials*, 12(2019), No. 14, art. No. 2224.
- [40] W.Y. Luo, Y.Z. Liu, and J.J. Shen, Effects of binders on the microstructures and mechanical properties of ultrafine WC–10%Al<sub>x</sub>CoCrCuFeNi composites by spark plasma sintering, *J. Alloy. Compd.*, 791(2019), p. 540.
- [41] R.Z. Chen, S. Zheng, R. Zhou, et al., Development of cemented carbides with Co<sub>2</sub>FeNiCrCu high-entropy alloyed binder prepared by spark plasma sintering, *Int. J. Refract. Met. Hard Mater.*, 103(2022), art. No. 105751.
- [42] P.L. Zhou, D.H. Xiao, P.F. Zhou, Y.X. Yu, and M.H. Yuan, Microstructure and properties of ultrafine-grained WC–Al<sub>x</sub>CrFeCoNi composites prepared by hot pressing, *Mater. Sci. Eng. Powder Metall.*, 24(2019), No. 2, p. 100.
- [43] D.H. Zheng and Y. Tang, Preparation and research of high-entropy-alloy CoCrFeNiTiAl bonded WC cemented carbide, *Powder Metall. Ind.*, 32(2022), No. 6, p. 16.